that yield consistent and radiogenic initial Nd isotope ratios and trace-element patterns characteristic of mid-ocean ridge melts. Other selection criteria include using trace-element data for rocks with high MgO (>6 wt%) to eliminate the possibility of oxide-induced fractionation of Nb versus Th and U [Y. Niu, K. D. Collerson, R. Batiza, J. I. Wendt, M. Regelous, *J. Geophys. Res.*, in press] and using suites believed to be of volcanic origin (rather than cumulates) to avoid Th/U fractionation caused by crystallization processes. From these criteria, the best datasets are derived from uncontaminated Archaean to early Proterozoic komatiites, komatiitic basalts, and basalts; post-Archaean obducted normal (N-MORB) or enriched (E-MORB) MORB ophiolites; tectonically emplaced intraoceanic arcs; and some uncontaminated continental mafic volcanics (Table 1). Three Th/U ratios were also calculated from initial $^{208}Pb/^{204}Pb$ and $^{206}Pb/^{204}Pb$ isotope data of other mantle-derived rocks. The standard deviations of most individual datasets are between ~5 and 10%. This is significantly smaller than the total variation in the ratio over geological time. The means of individual datasets of the same age are in excellent agreement (Table 1). Because we compare relative changes of elemental ratios, our conclusions are not impaired by the slight differences in the bulk distribution coefficients of the three elements.

8. C. J. Allègre and E. Lewin, *Earth Planet. Sci. Lett.* **96**, 61 (1989).
9. J. D. Kramers and I. N. Tolstikhin, *Chem. Geol.* **139**, 75 (1997).
10. The mean Nd isotope mantle extraction age of continental crust is between 2.0 and 2.2 Ga [S. R. Taylor and S. M. McLennan, *Rev. Geophys.* **33**, 241 (1995); S. L. Goldstein, R. K. O'Nions, P. J. Hamilton, *Earth Planet. Sci. Lett.* **70**, 221 (1984)].
11. I. J. Duncan, *J. Geodyn.* **2**, 1 (1985); R. E. Zartman and S. Haines, *Geochim. Cosmochim. Acta* **52**, 1327 (1988); M. T. McCulloch, *Earth Planet. Sci. Lett.* **115**, 89 (1993).
12. H. Staudigel, G. R. Davies, S. R. Hart, K. M. Marchant, B. M. Smith, *Earth Planet. Sci. Lett.* **130**, 169 (1995).
13. Y. Asmerom and S. B. Jacobsen, *ibid.* **115**, 245 (1993); P. S. Andersson, G. J. Wasserburg, J. H. Chen, D. A. Papanastassiou, J. Ingri, *ibid.* **130**, 217 (1995); D. Mathieu, M. Bernat, D. Nahon, *ibid.* **136**, 703 (1995).
14. R. Stalder, S. F. Foley, G. P. Brey, I. Horn, *Geochim. Cosmochim. Acta* **62**, 1781 (1998); J. M. Brenan, H. F. Shaw, D. L. Phinney, F. J. Ryerson, *Earth Planet. Sci. Lett.* **128**, 327 (1994); J. Ayers, *Contrib. Mineral. Petrol.* **132**, 390 (1998).
15. A. Reymer and G. Schubert, *Tectonics* **3**, 63 (1984).
16. J. D. Kramers, T. F. Nägler, I. N. Tolstikhin, *Schweiz. Mineral. Petrogr. Mitt.* **78**, 169 (1998); T. F. Nägler and J. D. Kramers, *Precambrian Res.* **91**, 233 (1998).
17. Averages of Angozero suite [I. S. Puchtel *et al.*, *Contrib. Mineral. Petrol.* **130**, 134 (1998)] quoted in Table 1 omitted samples 89103 and 9112 because of aberrant Th/U ratios.
18. J. Gutzmer and N. J. Beukes, *Geology* **26**, 263 (1998); A. E. Isley, *J. Geol.* **103**, 169 (1995).
19. Average of Deep Sea Drilling Project Legs 28 and 29 is from D. G. Pyle, D. M. Christie, J. J. Mahoney, and R. A. Duncan [*J. Geophys. Res.* **100**, 22261 (1995)]. The Th/U data is from old Western Indian Ocean [J. J. Mahoney *et al.*, *J. Petrol.* **39**, 1285 (1998)].
20. J. Dostal and B. N. Church, *Geol. Mag.* **131**, 243 (1994).
21. J. D. Keppie and J. Dostal, *ibid.* **135**, 171 (1998). Sample 191A was rejected due to high Th concentration.
22. K. S. Lee, H. W. Chang, K. H. Park, *Precambrian Res.* **89**, 47 (1998).
23. Average of dyke complex samples is from J. Dostal, C. Dupuy, and R. Caby [*ibid.* **65**, 55 (1994)].
24. M. Zimmer, A. Kröner, K. P. Jochum, T. Reischmann, W. Todt, *Chem. Geol.* **123**, 29 (1995). Basalt average was calculated without samples GG72, GG184, and GG172, for which U disturbance is inferred; gabbro average was calculated from samples GG77, GG82, GG87, and GG88 (only used for Nb/Th ratios).
25. Average of E-MORB is from R. A. Stern, E. C. Syme, and S. B. Lucas [*Geochim. Cosmochim. Acta* **59**, 3131 (1995)].
26. The Th/U ratio was calculated from Pb isotope systematics [N. T. Arndt and W. Todt, *Chem. Geol.* **118**, 9 (1994)].
27. Average of transitional basalts with Th concentration lower than 0.35 ppm is from M. I. Leybourne, N. A. van Wagoner, and L. D. Ayres [*J. Petrol.* **38**, 1541 (1997)].
28. P. Peltonen, A. Kontinen, H. Huhma, *ibid.* **37**, 1359 (1996).
29. Averages of spinifex textured komatiites for Abitibi and Barberton are from Y. Lahaye *et al.* [*Chem. Geol.* **126**, 43 (1995)].
30. Average of komatiite, spinifex-komatiite, and komatiitic basalt is from J. Fan and R. Kerrich [*Geochim. Cosmochim. Acta* **61**, 4723 (1997)].
31. Average of komatiites and Fe basalts is from Q. Xie, R. Kerrich, and J. Fan [*ibid.* **57**, 4111 (1993)].
32. Average of komatiites and basalts is from J. Dostal and W. U. Mueller [*J. Geol.* **105**, 545 (1997)].
33. J. A. Ayer and D. W. Davis, *Precambrian Res.* **81**, 155 (1997). Only least-contaminated samples 84-610, 93-22, 89-110, 87-838, and 87-839 from lower Keewatin were used.
34. Average of all komatiites and basalts is from K. Y. Tomlinson *et al.* [*ibid.* **89**, 59 (1998)]. Sample KYT376 was rejected due to high Th concentration (1.61 ppm).
35. Time-integrated Th/U ratio based on Pb isotopes is from A. H. Wilson and R. W. Carlson [*Earth Planet. Sci. Lett*, **96**, 89 (1989)].
36. Average of Archean-MORB basalts is from H. Ohta, S. Maruyama, E. Takahashi, Y. Watanabe, and Y. Kato [*Lithos* **37**, 199 (1996)]. Samples CLG-10 and CLG-12.H were excluded.
37. B. S. Kamber and S. Moorbath, *Chem. Geol.* **150**, 19 (1998). The Th/U ratio of depleted mantle is derived from least-radiogenic silicate Pb isotope ratios on Earth.
38. K. D. Collerson, unpublished data.
39. This work could not have been done without the high-quality datasets published by our colleagues. Research on crustal evolution by K.D.C. was supported by NSF and the Australian Research Council. B.S.K. is funded by Swiss National Science Foundation grant 8220-050352.

2 November 1998; accepted 25 January 1999

# Rapid Thinning of Parts of the Southern Greenland Ice Sheet

**W. Krabill,[1]* E. Frederick,[2] S. Manizade,[2] C. Martin,[2] J. Sonntag,[2] R. Swift,[2] R. Thomas,[2] W. Wright,[1] J. Yungel[2]**

**Aircraft laser-altimeter surveys over southern Greenland in 1993 and 1998 show three areas of thickening by more than 10 centimeters per year in the southern part of the region and large areas of thinning, particularly in the east. Above 2000 meters elevation the ice sheet is in balance but thinning predominates at lower elevations, with rates exceeding 1 meter per year on east coast outlet glaciers. These high thinning rates occur at different latitudes and at elevations up to 1500 meters, which suggests that they are caused by increased rates of creep thinning rather than by excessive melting. Taken as a whole, the surveyed region is in negative balance.**

The mass balance of the polar ice sheets is clearly important to global sea level, but it is still not known whether the Greenland and Antarctic ice sheets are increasing or decreasing in size. Mass balance can be inferred directly by comparing repeated aircraft or satellite altimeter surveys over periods of a few years, giving an indication of the change in volume over the survey intervals. Recent analyses of Seasat and Geosat radar-altimeter data over southern Greenland (*1*) indicate average thickening between 2 and 4 cm/year at elevations above 2000 and 1700 m, respectively, for the period 1978–1988 at latitudes less than 72°N. Because of limitations associated with the satellite instruments, there are few useful data below elevations of 2000 m and scarcely any below 1700 m. Here, we present results from aircraft laser-altimeter measurements of elevation change over all of southern Greenland, including first estimates for the peripheral regions, which represent about 40% of the ice sheet area and are likely to be most susceptible to climate change.

In 1993 and 1994, NASA surveyed the entire Greenland ice sheet by airborne laser altimetry, obtaining surface-elevation profiles with root mean square (rms) accuracy of 10 cm or better (*2*) along flight lines that crossed all the major catchment basins. In 1998, the 10 flight lines flown in 1993 in the south of Greenland were resurveyed with about 99% repeat coverage; the flight lines in the north will be resurveyed in 1999.

The airborne topographic mapper (ATM) is a conical-scanning laser ranging system with a pulse repetition rate of 3 kHz (800 Hz in 1993) and a scan rate of 10 Hz (5 Hz), at an off-nadir angle of 10°. Aircraft location was determined by kinematic global positioning system (GPS) techniques, and aircraft heading, pitch, and roll were measured by inertial navigation systems. At an aircraft altitude of 400 m above the surface, the ATM obtained measurements of the surface elevations for many 1-m footprints within a 140-m-wide swath, with average sep-

[1] Laboratory for Hydrospheric Processes, NASA Goddard Space Flight Center, Wallops Flight Facility, Building N-159, Wallops Island, VA 23337, USA. [2] EG&G Services, Wallops Flight Facility, Building N-159, Wallops Island, VA 23337, USA.

*To whom correspondence should be addressed. E-mail: krabill@osb.wff.nasa.gov

aration between footprints of about 2 m (4 m in 1993). Instrument biases and overall performance were checked during each flight by overflying flat surface areas (such as sea ice or fjords) and precisely surveyed portions of the runway. Additional checks on data consistency were made by comparing surface elevations at locations where flight lines cross and at stations on the ice sheet where surface-based GPS measurements were made (*2*). During the repeat survey, the airplane was navigated along the earlier flight lines by a GPS-guided autopilot (*3*), achieving cross-track separations typically less than 50 m.

Most of the ice sheet is sufficiently smooth for the 140-m-wide ATM data swath to be well described by a series of 70-m square planes (platelets) that best fit the data acquired on each side of the flight track. Data from different flights were compared by seeking the closest platelet from the second flight with its center lying within 75 m of the center of a platelet from the first flight and comparing heights that had been interpolated to the point midway between the two platelet centers by taking account of the platelet slopes. The plane-surface approximation introduces random errors to the derived elevation changes, but these errors generally are small and can be minimized by averaging comparisons along the flight line. The rms fit of the measured surface elevations to these platelets was typically 5 cm or better and, for most purposes, the platelets adequately represent the information contained within the laser data while reducing the data volume significantly. Where the surface is rough, such as on outlet glaciers, the elevation at each laser footprint from one flight was compared with elevations at all footprints from the second flight that lie within a 1-m search radius.

To estimate errors in computed elevation change rates, we note that comparison of platelet elevations at flight-line crossing points from the same year gives rms differences of about 10 cm, partly caused by errors that are systematic to a flight. Consequently, systematic errors for an individual flight could be as high as 7 cm, yielding a possible bias in estimated elevation change from 1993 to 1998 of about 10 cm along each flight line, or 2 cm/year. This should be independent of errors for the other nine flight lines, so that errors in change rates averaged over a region containing many flight lines decrease to as little as 0.6 cm/year. Additional errors in each survey, associated primarily with a 1-cm uncertainty in the location of the GPS base station, introduce a systematic bias in change rates of <0.3 cm/year, increasing the error in average change rates derived from all 10 flight lines to 0.7 cm/year.

Estimated rates of elevation change are shown in Fig. 1, with regional trends derived by interpolating between flight lines. Interpolation is most reliable above 2000 m, where there are many flight lines. Figure 1 shows the rates of change in surface elevation that occurred between June–July 1993 and June–July 1998. Because rock beneath the ice sheet is also moving vertically as a result of past and present changes in ice loading, these are not identical to ice thickening and thinning rates. Consequently, a rock uplift rate of about 0.5 cm/year (*1*) should be subtracted from our elevation-change rates to yield estimated ice thickening and thinning rates.

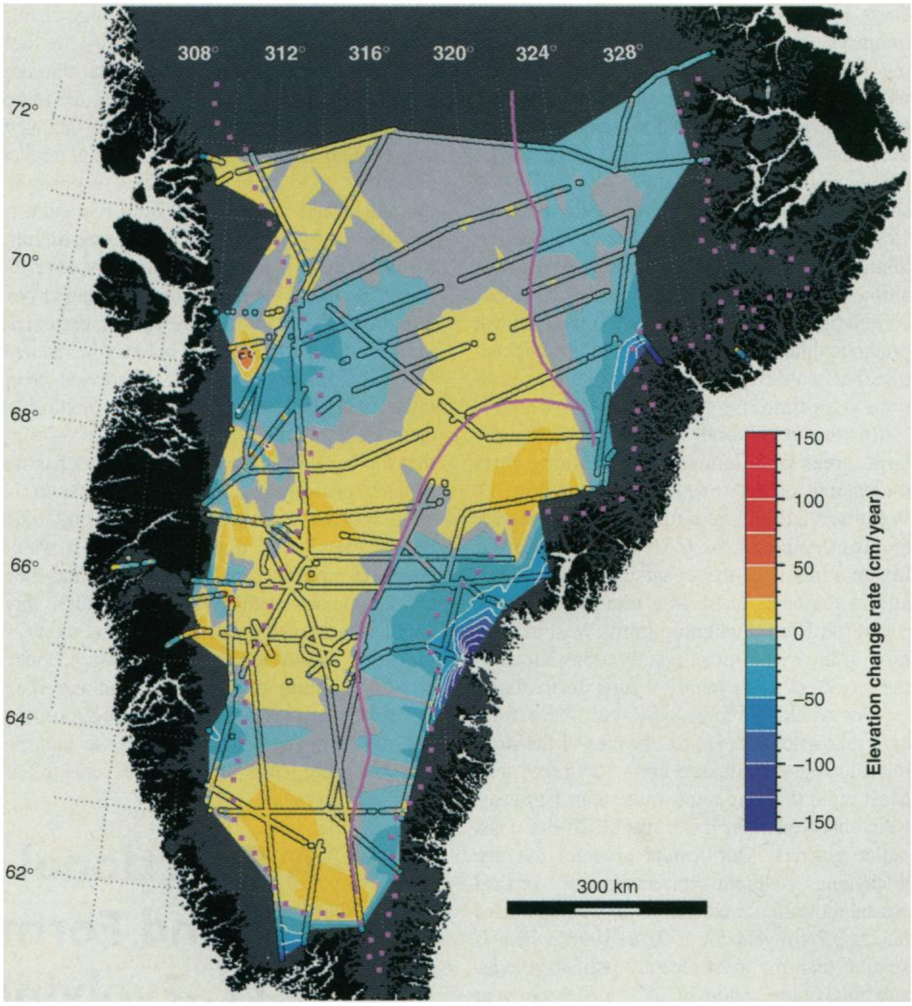


**Fig. 1.** Southern Greenland, showing flight tracks (outlined in black) of laser-altimeter surveys color-coded according to the rate of change in surface elevation. Pale gray segments are in balance within the survey errors (±2 cm/year). Regional rates of surface elevation change were obtained by interpolating between the flight-track data. The line of the ice-sheet ridge is pink, and the 2000-m elevation contour is marked by pink dots.

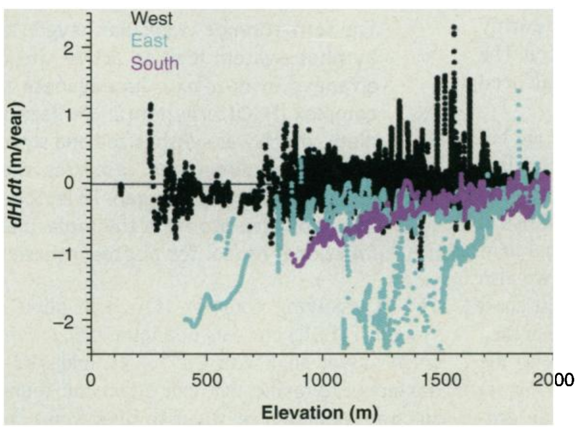


**Fig. 2.** Ice thickening and thinning rates (*dH/dt*) plotted against surface elevation for regions below 2000 m for the east, south, and west coastal regions. There is both thickening and thinning along the west side of the ice sheet, averaging almost exactly to zero, but there is major thinning almost everywhere in the east and south.

Three areas in the south are thickening at rates of up to 25 cm/year (centered near 68°N 319°E, 67°N 314°E, and 63°N 313°E in Fig. 1). The two northernmost of these show reasonable agreement with results from satellite radar-altimeter data (*1*), with thickening rates in the east increasing to more than 15 cm/year nearer the coast. In the south, thickening rates reach maximum values of 25 cm/year. All three thickening zones are in regions of high snowfall (*4*), with accumulation rates strongly linked to storm intensity and subject to considerable interannual variability. However, model studies (*4*) conclude that precipitation over this region should have decreased significantly between 1985 and 1995, which would have resulted in thinning. In the northwest, where repeat radar-altimeter data (*1*) and comparison of snow accumulation with ice discharge (*5*) have shown previous thinning, we observe a slight thickening. This could represent a change in conditions with time.

In the peripheral regions, we observe large areas of thinning, with thinning rates increasing rapidly toward the ocean (Fig. 1). We observe thinning of up to 20 cm/year over an area centered near 69°N 313°E and at far higher rates near the coast in the southwest and in the east. There is a remarkably sharp transition from thickening in the west to thinning in the east almost exactly along much of the ice-sheet ridge where it runs north-south.

Our results agree broadly with those from radar-altimeter data (*1*) for the east of the summit ridge but include data from a far larger area. Most rapid thinning rates (more than 1 m/year) were observed in the lower reaches of east coast outlet glaciers. Our results give an average thickening (without correcting for vertical crustal motion), for elevations above 2000 m, of $0.5 \pm 0.7$ cm/year for 1993 to 1998, which is smaller than the most recently published average thickening value of $2.2 \pm 0.9$ cm/year between 1978 and 1988 estimated from satellite radar-altimeter data for the same region (*1*). However, neither of the error estimates includes errors associated with interpolating between flight lines, and that for the radar-altimeter data includes only the random component of the error (*1*). Consequently, these higher elevation central regions could have been almost exactly in balance for the past 20 years, or they could be shifting from slight thickening to a balanced condition.

The lower elevation coastal regions are behaving differently. Thickening and thinning rates for all surfaces below 2000 m show extensive thinning in the east (Fig. 2), consistent with observations of warmer than normal temperatures for 1993 to 1998. However, we also observed areas of thinning near the west coast (Fig. 1), where many locations were cooler than normal (*6*). The elevation changes along the west and south sides of the ice sheet (Fig. 1) show good qualitative agreement with estimates of marginal ice advance and retreat between 1950 and 1985 based on comparison of aerial photographs (*7*), but not along the east coast, where the earlier, rather sparse data suggest glacier advance between 1950 and 1985.

We observed the highest rates of thinning in the lower reaches of outlet glaciers along the east coast, where we might expect large changes caused by interannual variability in melt rates (*8*). Over the 5-year period, total thinning of as much as 10 m was observed in the lower reaches of all east coast outlet glaciers that were surveyed, at latitudes up to 69°N and at surface elevations up to 1500 m (Fig. 2). The observed thinning could be explained by a reduction in snowfall or by an increase in summer melting of as much as a 10-m ice equivalent over the 5-year period. This represents a sustained perturbation of 100% or more and is extremely unlikely. Consequently, we believe the glaciers to be thinning as a result of increased creep rather than because of excessive melting or decreased snowfall. This raises the possibility that the basal friction of these glaciers has decreased, possibly because of an increase in the amount of surface melt water penetrating to the bed of the glacier. If this is correct, it would represent a mechanism for transfer of ice-sheet mass to the oceans that is potentially larger than could be achieved by surface melting alone.

These observations of extensive, near-coastal thinning of the Greenland ice sheet illustrate the importance of detailed monitoring of these regions. The airborne surveys reported here, and those to be repeated in 1999, will establish baseline data sets, which will be extended with information from NASA's ICESAT (*9*). This satellite laser altimeter will be launched in 2001 to measure ice-surface elevations in Greenland and Antarctica at all latitudes up to 86°.

### References and Notes


1. C. H. Davis, C. A. Kluever, B. Haines, *Science* **279**, 2086 (1998); H. J. Zwally, A. C. Brenner, J. P. DiMarzio, *ibid.* **281**, 1251 (1998).
2. W. B. Krabill, R. H. Thomas, C. F. Martin, R. N. Swift, E. B. Frederick, *Int. J. Remote Sens.* **16**, 1211 (1995).
3. C. W. Wright, *Proc. SPIE Conference*, Orlando, FL (Bellingham, Washington, DC, 1992), pp. 2–7.
4. D. H. Bromwich *et al.*, *J. Geophys. Res. Atmos.* **103**, 26007 (1998).
5. R. H. Thomas *et al.*, *J. Glaciol.*, in press.
6. W. Abdalati, personal communication (October 1998). Summer temperatures (June, July, and August) were averaged for 1993 to 1997 and compared with average summer temperatures for 1979 to 1997 to show an increase on the east coast of about 0.3°C and a similar decrease along much of the west coast. Data from 19 coastal stations were used.
7. A. Weidick, *Rapp. Gronlands. Geol. Unders.* **152**, 73 (1991).
8. R. J. Braithwaite, *Global Planet. Change* **9**, 251 (1994).
9. Schutz, B., *Proc. Wegener-98*, Krokkleiva, Norway (Norwegian Mapping Authority, Hønefoss, Norway, 1998).


10. Supported by NASA's Polar Research Program and ICESAT Project. We thank the crew of the NASA P-3 aircraft used for the Greenland surveys, W. Abdalati for analysis of Greenland coastal meteorological data for temperature trends, and C. H. Davis and H. J. Zwally for providing their latest results from analysis of satellite radar-altimeter data. We wish to acknowledge the outstanding technical support of R. Mitchell, A. Waller, and J. Scott.

26 October 1998; accepted 2 January 1999


# A Functional Model for O–O Bond Formation by the $O_2$-Evolving Complex in Photosystem II


**Julian Limburg,[1] John S. Vrettos,[1] Louise M. Liable-Sands,[2] Arnold L. Rheingold,[2] Robert H. Crabtree,[1]* Gary W. Brudvig[1]***



**The formation of molecular oxygen from water in photosynthesis is catalyzed by photosystem II at an active site containing four manganese ions that are arranged in di-μ-oxo dimanganese units (where μ is a bridging mode). The complex $[H_2O(terpy)Mn(O)_2Mn(terpy)OH_2](NO_3)_3$ (terpy is 2,2′:6′,2″-terpyridine), which was synthesized and structurally characterized, contains a di-μ-oxo manganese dimer and catalyzes the conversion of sodium hypochlorite to molecular oxygen. Oxygen-18 isotope labeling showed that water is the source of the oxygen atoms in the molecular oxygen evolved, and so this system is a functional model for photosynthetic water oxidation.**


The $O_2$-evolving complex (OEC) in photosystem II (PSII) consists of a tetranuclear Mn cluster associated with $Ca^{2+}$, $Cl^-$, and a redox-active tyrosine that can effect the four-electron oxidation of water to dioxygen (*1*). Extended x-ray absorption fine structure studies have shown that the Mn tetramer is made up of di-μ-oxo dimeric Mn units (μ is a bridging mode) (*2*). This assignment was made by a comparison with structural model